

Secondary-phase orientation probed by EPR: Y_2BaCuO_5 in $\text{YBa}_2\text{Cu}_3\text{O}_{7-x}$

N. Pellerin, P. Simon, P. Odier, F. J. Gotor, N. J. Poirot, and L. Vutien
Centre de Recherches sur la Physique des Hautes Températures, CNRS, 45071 Orléans Cedex 2, France

L. Durand

*Commissariat à l'Énergie Atomique, Centre d'Études et de Recherches sur les Matériaux, Département de Technologie des Matériaux,
 Section de Recherches de Métallurgie Physique, CEN de Saclay, 91191 Gif sur Yvette Cedex, France*

I. Monot

Cristallographie et Sciences des Matériaux—ISMRA, 14050 Caen Cedex, France

(Received 12 June 1996)

Textured $\text{YBa}_2\text{Cu}_3\text{O}_{7-x}$ samples have been studied by electronic paramagnetic resonance. EPR spectroscopy allows us to analyze the Y_2BaCuO_5 second phase present as inclusions in the $\text{YBa}_2\text{Cu}_3\text{O}_6$ textured matrix. All samples were deoxygenated in order to limit the skin effect due to conductivity. This is applied to samples textured according to different techniques. Preferential orientation of these particles according to the 123 matrix can be observed. For instance, if texturing under a magnetic field, the particular Y_2BaCuO_5 orientation is observed of the \mathbf{b}_{211} axis ($b=7.132 \text{ \AA}$) parallel to \mathbf{c}_{123} and to the magnetic field direction. By appropriate calculations from initial spectra, the fraction of preferred orientation of these Y_2BaCuO_5 grains can be quantified. This orientation comprises $16 \pm 2\%$ of the Y_2BaCuO_5 weight for texturing under a magnetic field, presently one of the highest values obtained. It involves the longest size of Y_2BaCuO_5 elongated grains lying in $\text{YBa}_2\text{Cu}_3\text{O}_6$ planes, facilitating the texturation process. Texturing on Y_2O_3 by the modified melt textured growth method leads to a preferential orientation of Y_2BaCuO_5 grains too, but in another direction, i.e., \mathbf{b}_{211} perpendicular to \mathbf{c}_{123} . There is no Y_2BaCuO_5 preferential orientation if texturing with a thermal gradient or on a monocrystalline MgO substrate. This type of analysis can be applied easily to other systems (nanocomposites, dispersoids, etc.), providing that the signal of the secondary phase can be clearly separated from the signal of the primary one. [S0163-1829(97)06001-3]

I. INTRODUCTION

High- T_c cuprates are EPR silent above and below T_c .¹ The presence of bidimensional antiferromagnetic fluctuations has been proposed^{2,3} to explain this, but no definite conclusions are yet possible. The second phase could be then attractively studied by this technique. CuO which is often present as an impurity in textured $\text{YBa}_2\text{Cu}_3\text{O}_{7-x}$ (123) gives no visible EPR signal in X band, or very broadband.¹ The EPR signal of the BaCuO_{2+x} phase, also present in small quantity, strongly depends on oxygen stoichiometry.⁴ For small x values it consists of a very broad line, while when oxidized the line shape is closer to that of Y_2BaCuO_5 (211). However, due to its more marked rhombic character, it is definitely different from that of 211.⁵ Moreover, its smaller intensity than that of 211 allows one to neglect its contribution in 123 based compounds. Then EPR allows one to study the 211 secondary phase trapped in the 123 textured matrix.⁶ This spectroscopy gives access to bulk information on 211 phase, contrary to TEM, often used to study 123/211 interfaces.

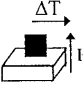
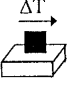
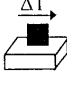
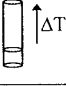
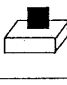
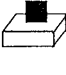
Various methods allow one to elaborate bulk high- T_c superconducting materials.^{7,8} Melt texturing is one of the most promising for 123.⁹ Its peritectic decomposition into the green phase 211 plus a liquid, followed by a slow cooling, allows directional growth of 123 domains. As a result of kinetic limitations, the peritectic recombination of 211 into 123 is not complete which causes 211 inclusions to remain

trapped in the texture. The presence of 211 grains in the 123 matrix involves various defects which increase the flux pinning. However, the exact pinning mechanisms are still a matter of debates. Because 211 is a witness of the peritectic decomposition and recrystallization of 123, it is a key factor for both crystallization process understanding and critical current enhancement. Its chemical and physical characterization is therefore an essential step in the development of these materials. Electron microprobe,¹⁰ SEM, and TEM are now systematically used. Here we have exploited EPR as a way to probe the orientation of 211 inclusions with respect to the matrix. It is a rare example of such a spectroscopy applied to a second-phase analysis.

The 211 phase is insulating and has an EPR signal due to the presence of magnetically independent Cu^{2+} ions with 1/2 spin. The only determination of the principal axes of the g tensor of the Cu^{2+} ion in the 211 phase has been made by Kobayashi *et al.*,⁵ on single crystals. They have obtained the values $g_x=2.050$, $g_y=2.094$, and $g_{\parallel}=g_z=2.222$, corresponding to a local rhombic symmetry. Because of a very low splitting between g_x and g_y , the mean value is noted g_{\perp} . Moreover, the principal (X, Y, Z) g -tensor axes are respectively parallel to the crystallographic ($\mathbf{a}, \mathbf{c}, \mathbf{b}$) axis where $a=5.658 \text{ \AA}$, $b=7.132 \text{ \AA}$, and $c=12.181 \text{ \AA}$. This result is consistent with our x-ray pole figure on 211.^{11,12} The \mathbf{a} crystallographic axis lies parallel to the longest dimension of the elongated particles with a typical size of less than $20 \mu\text{m}$.

In previous papers, we have reported qualitative EPR re-

TABLE I. Synthesizing conditions, and EPR results: preferential orientation and weight fraction of oriented 211.

Samples	Initial composition	EXTERNAL PARAMETERS		SUBSTRATE AND CONFIGURATION				EPR MEASUREMENTS	
		H Field	Thermal gradient	Zone melting	211 polycrystal	Y2O3 polycrystal	MgO single crystal	Preferred Orientation	%211 Oriented $\pm 2\%$
A	123+20wt%211 sol gel	4T	30°C/cm					$b_{211} // c_{123}$	16
B	123+20wt%211 sol gel	0	30°C/cm						0
C	123 Rhône-Poulenc	0	20°C/cm					$b_{211} \perp c_{123}$	1
D	123 Hoechst	0	60°C/cm						0
E	123 Hoechst	0	0						0
F	123 Hoechst	0	0					$b_{211} \perp c_{123}$	4

sults on 211 inclusions partially oriented according to the 123 matrix. Curiously, the orientation is process dependent.^{6,11,12} In particular, samples textured on the Y_2O_3 substrate without thermal gradient and by a modified MTG (melt textured growth) method⁶ give a substantial orientation of 211 grains such that the b_{211} axis lies in $(ab)_{123}$ planes. This particular orientation was also evidenced by microstructural analysis of 123/211 interfaces.¹³ We have proved elsewhere that a magnetic field applied during the high temperature part of the thermal process induces another 211 particular orientation, i.e., b_{211} parallel to c_{123} , and parallel to the magnetic field direction.^{11,12} This result has been confirmed by x-ray pole figures on the secondary 211 phase.¹² One can then expect a noticeable magnetic susceptibility anisotropy of 211 phase, as in 123.^{14,15}

The present paper reports a quantitative study of the fraction of nonrandomly oriented 211 inclusions in 123 textured materials. This method has been applied to samples textured with various processes, i.e., different substrates, with or without a thermal gradient, with or without application of a magnetic field. The orientation features and the fraction of 211 oriented grains are discussed as a function of these different experimental conditions. Our results allow a better understanding of the properties of residual 211, and of texturation mechanisms.

II. EXPERIMENT

A. Samples

Samples of various origins have been studied (Table I). Samples A and B have been prepared by horizontal direc-

tional cooling with an applied vertical magnetic field in case A. The method has been described elsewhere.^{12,16} Sample C has been prepared by horizontal directional cooling on a polycrystalline Y_2BaCuO_5 substrate.¹⁷ Samples D, E, and F have been elaborated by two of us (N.P. and L.V.). Sample D has been vertically zone melted at 1030 °C with a translation rate of 1 mm/h. The heater was a metal ring. Samples E and F have been textured with a MTG modified method on different substrates.⁶ Sample G is a sintered ceramic composed of 123 with 10 wt. % added 211.

B. EPR

All spectra were obtained on a Bruker ER200D spectrometer, working in X band ($\nu \approx 9.7$ GHz). They were recorded at room temperature in air. For insulating samples, the doubly integrated EPR spectrum is proportional to the number of spins resonating in the cavity, provided the linewidths are not too large. In conducting samples, this is not necessarily the case: due to dispersion of the microwave in the sample (skin effect), the hf magnetic field is not homogeneous in the sample volume, leading to the well-known Dysonian line shapes.^{18,19} One way of treating this problem is to consider the experimental EPR spectrum composed not only from the derived absorption, i.e., imaginary part χ'' of the magnetic susceptibility, but including also the contribution of the derived dispersion, i.e., the real part of the susceptibility χ' . Following Pake *et al.*,^{20,21} this double contribution can be sketched up for an ideal Lorentzian EPR line. Figure 1 displays the derived absorption and dispersion vs magnetic field in this case, corresponding to their contribution to the EPR spectrum (α in Fig. 1 is an arbitrary parameter). One sees

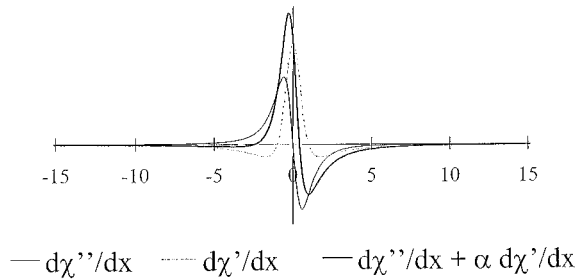


FIG. 1. First derivative of χ' and χ'' versus x , where x is a dimensionless variable corresponding to the field H . Addition of both these contributions reflects the EPR signal in conducting compounds.

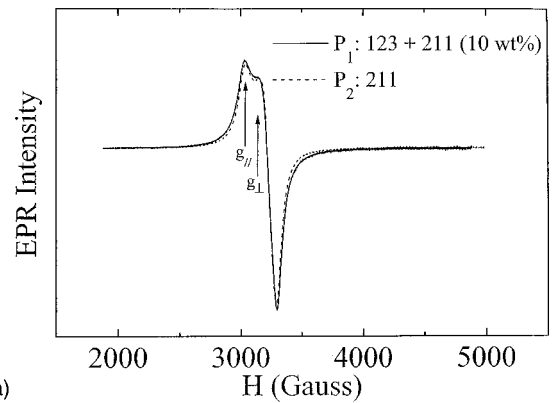
that the dispersion part leads to an asymmetry of the signal which precludes any integration of the absorption part and thus any precise estimation of the number of spins.

Samples studied by EPR are single domains selected by cleavage along $(ab)_{123}$ planes in textured samples. They must be of small size (about $1 \times 2 \times 0.5 \text{ mm}^3$) and deoxygenated to reduce their conductivity, and thus to suppress the major part of the dispersion contribution to the EPR spectra. The samples are heated at 800°C during 5 h in argon flux, and slowly cooled to RT in the same atmosphere. Oxygen stoichiometry is thus lowered to 6.0–6.1 according to thermogravimetric analysis (TGA) measurements. The corresponding resistivity is in the range of $150 \text{ m}\Omega \text{ cm}$ ($\text{YBa}_2\text{Cu}_3\text{O}_6$), involving a skin depth in X band of approximately $200 \mu\text{m}$ while it is only $20 \mu\text{m}$ in $\text{YBa}_2\text{Cu}_3\text{O}_7$.

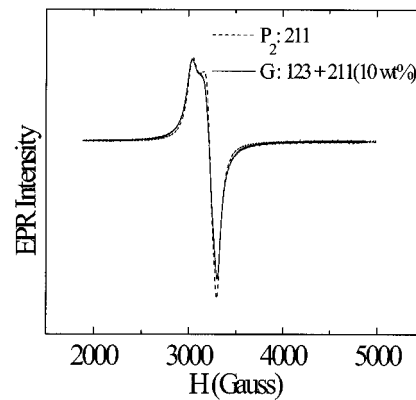
The samples are fixed with vacuum grease on an altuglass rod inside the EPR cavity. Their (ab) planes can be placed either horizontally or vertically, and they can be rotated around the vertical axis. All orientations of the principal planes vs magnetic field can then be chosen. Any preferential orientation of the 211 phase would involve changes in the spectrum shape upon rotating the textured sample. On the contrary, in 211 powders and in samples with isotropic 211 orientation, the spectrum will be evidently angular independent.

C. Quantifying the ratio of nonrandomly oriented 211

To calculate the percentage of nonrandomly oriented 211 spins in a deoxygenated textured sample, two spectra recorded at two particular angle values are used: the spectrum which has the maximum intensity at g_{\parallel} and the minimum intensity at g_{\perp} , and the spectrum at 90° of the previous one with minimum at g_{\parallel} and maximum at g_{\perp} . In a first step, these two particular spectra are integrated to obtain absorption signal vs magnetic field. In a first approximation, their surface is proportional to the total Cu^{2+} spin number of 211 phase, and then to the 211 phase amount. We normalize the surfaces to consider the same total spin number in both spectra. This new value is denoted S . The difference between the 2 integrated spectra is made: this provides a graph having a positive part equal to its negative counterpart. The corresponding area, denoted σ , is proportional to the oriented Cu^{2+} spin number of the 211 phase, then to the weight w of oriented 211. So the percentage of oriented 211 is simply



(a)



(b)

FIG. 2. EPR spectra of (a) powders: deoxygenated 123+10 wt. % 211 (P_1), and pure 211 powder (P_2); (b) pure 211 powder (P_2), and deoxygenated 123+10 wt. % 211 ceramic (G).

$$P = \% \text{ Cu}_{211}^{2+} \text{ oriented spins} = \frac{100\sigma}{S} = \frac{100w_{211(\text{oriented})}}{w_{211(\text{total})}}$$

D. Testing the method

Hanic *et al.*²² have shown a difference in EPR spectrum shapes between powdered and bulk conductor samples for $\text{YBa}_2\text{Cu}_3\text{O}_{6.9+x}$ wt. % Y_2BaCuO_5 ($1.7 < x < 68.8$). As a matter of fact, for such 123 stoichiometry, the skin depth is very reduced and the spectrum shape distortion by conductivity is strong. We have first checked that this is not the case for well deoxygenated samples.

For this purpose, deoxygenated powder $\text{YBa}_2\text{Cu}_3\text{O}_6+10$ wt. % Y_2BaCuO_5 (grain size $\leq 5 \mu\text{m}$), noted P_1 , and pure Y_2BaCuO_5 powder noted P_2 synthesized by a gel-derived method described elsewhere,²³ were prepared. Figure 2(a) displays EPR powders P_1 and P_2 spectra. P_1 powder has then been sintered at 800°C in Ar (grain size $\leq 20 \mu\text{m}$) to form a ceramic sample (noted G) of identical size ($1 \times 2 \times 0.5 \text{ mm}^3$) to that of textured samples. Figures 2(a) and 2(b) compare both spectra (P_1 and G) with pure 211 powder (P_2) spectrum. As expected, there is a very weak difference between them [Fig. 2(a)]. The difference between P_2 and G is less negligible [Fig. 2(b)]. The line of the sintered compound (G) exhibits a Dysonian character. Here the skin depth is about $200 \mu\text{m}$, so the microwave field does not penetrate uniformly the whole sample contrary to the powder.

It is useful to quantify the spectrum distortion due to conductivity from these reference samples. In the quantification

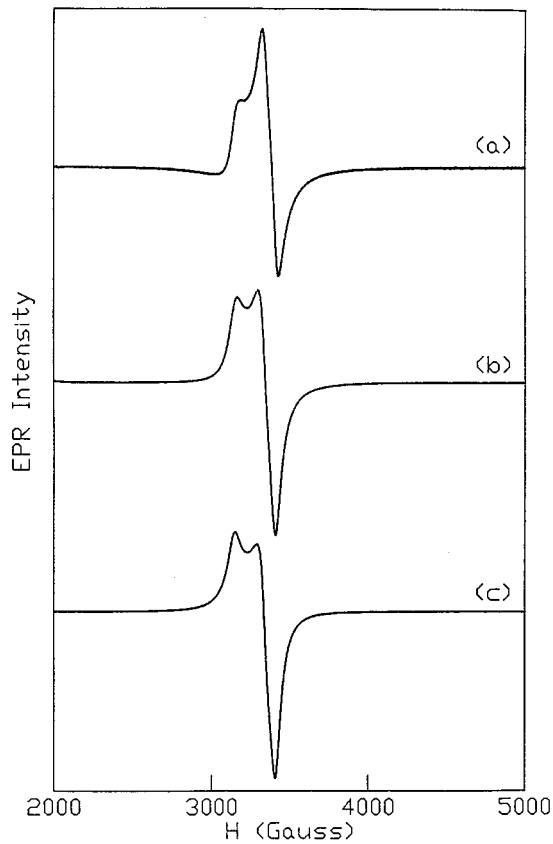


FIG. 3. EPR spectra dependence upon successive deoxygenations for sample *B* (textured under the magnetic field and thermal gradient). (a) As received, (b) partial deoxygenation ($O_{6.5}$), and (c) complete deoxygenation (O_6).

method of Sec. II C, the conductivity will lead to an error on the normalization of the absorption curves since the integral of the experimental spectrum is no more exactly the absorption spectrum. This can be estimated by calculating this on the *P1* powder (123+10 wt. % 211) and on the corresponding ceramic *G*. The difference between their integrated spectra gives an artifact value of σ attributed to the Dysonian profile of the ceramic spectrum. This value of σ will constitute the main source of the absolute error on the amount of oriented Cu_{211}^{2+} . It is significantly reduced on small and well deoxygenated samples and reaches 2 in percent unit. As a consequence, \mathcal{P} is measured within an error uncertainty of ± 2 .

III. RESULTS AND DISCUSSION

The Cu^{2+} signal in as-received textured ceramics differs significantly from that of well deoxygenated powders. As an example, Fig. 3 shows EPR signal dependence upon deoxygenation [(a)–(c)] for textured sample *B* in which no angular dependency can be evidenced. Figure 4 shows the corresponding integrated spectra; it will be commented on later. Figure 3(a) is typical of a conducting sample with Dysonian distortion: in particular a nonlinear base line can be noted together with a significantly reduced negative intensity contribution in the spectrum. This is qualitatively shown in Fig. 1 by summing up Lorentzian dispersion and absorption functions χ' and χ'' . Modeling the spectrum is presently very

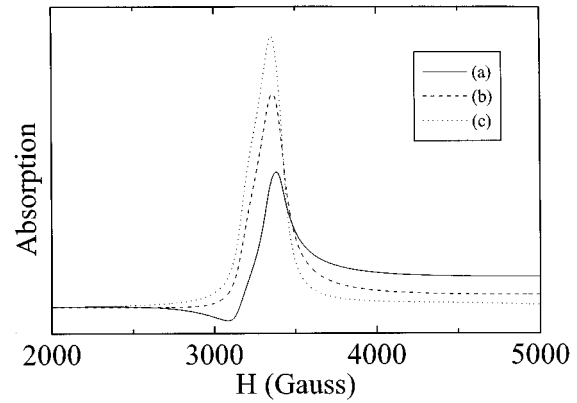


FIG. 4. Integrated spectra for sample *B*. (a) As received, (b) partial deoxygenation ($O_{6.5}$), and (c) complete deoxygenation (O_6). This figure shows the distortion effect due to Dysonian line shape on a sample with isotropic 211 orientation.

difficult and out of the scope of this brief paper. The fully deoxygenated ceramic, Fig. 3(c), shows an EPR signal identical to that of 211 powder [Fig. 2(a)].

Sample *A* shows orientational features in its EPR spectrum. Figure 5(a) displays the maximal intensity obtained when $(\mathbf{H}, \mathbf{c}_{123}) = 0$, i.e., maximum at g_{\parallel} for the continuous line and when $(\mathbf{H}, \mathbf{c}_{123}) = 90^\circ$, i.e., minimum at g_{\parallel} for the broken line. Despite a Dysonian line shape in this as-received sample, the nonrandom 211 spin orientation is clear in this sample. It is however necessary to deoxygenate it in order to get the exact amount of oriented spins. Figure 5(b) shows that skin effect will not be perceptible in this treated ceramic. The absorption associated to g_{\parallel} , then to the \mathbf{b}_{211} direction, is maximal when the field is along \mathbf{c}_{123} . Hence the preferred direction of \mathbf{b}_{211} in sample *A* is characterized by $\mathbf{b}_{211} \parallel \mathbf{c}_{123}$. We have not been able to detect any significant 211 orientation in the $(ab)_{123}$ plane, even by measuring in *Q* band (34 GHz), proving that the elongated 211 grains probably have their longest dimension (a_{211}) in the $(ab)_{123}$ plane in a “fiberlike” texture already observed by an x-ray pole figure.¹²

In order to get quantitative values of the oriented fraction integration of the spectra is requested. Absorption for sample *B* (no 211 orientation) is reported in Fig. 4. The Dysonian distortion has a clear signature in the as-received compound (see curve *a*, continuous line), while decreasing the conductivity by high temperature annealing in a neutral atmosphere completely suppresses the shift of the base line (see curve *c*, dotted line). Note the small asymmetry of the absorption line ascribed to the rhombic nature of the Cu^{2+} site in 211. Integration of EPR spectra for sample *A* presenting orientation of 211 is reported in Figs. 5(c) and 5(d). Figure 5(c) is for the as-received compound. A difference between orientations maximizing g_{\parallel} or g_{\perp} features is clear (respectively continuous and broken line), but a strong base line shift as in sample *B* is noticed. It is of the order of the magnitude of the absorption line and precludes any quantitative calculations of the oriented fraction. On the contrary, such a shift does not exist when the sample is deoxygenated [Fig. 5(d)]. Comparing Figs. 4 and 5(d) shows in a qualitative way the difference between an isotropic distribution of 211 particles and a partially oriented one. Clearly the pronounced shoulder of Fig.

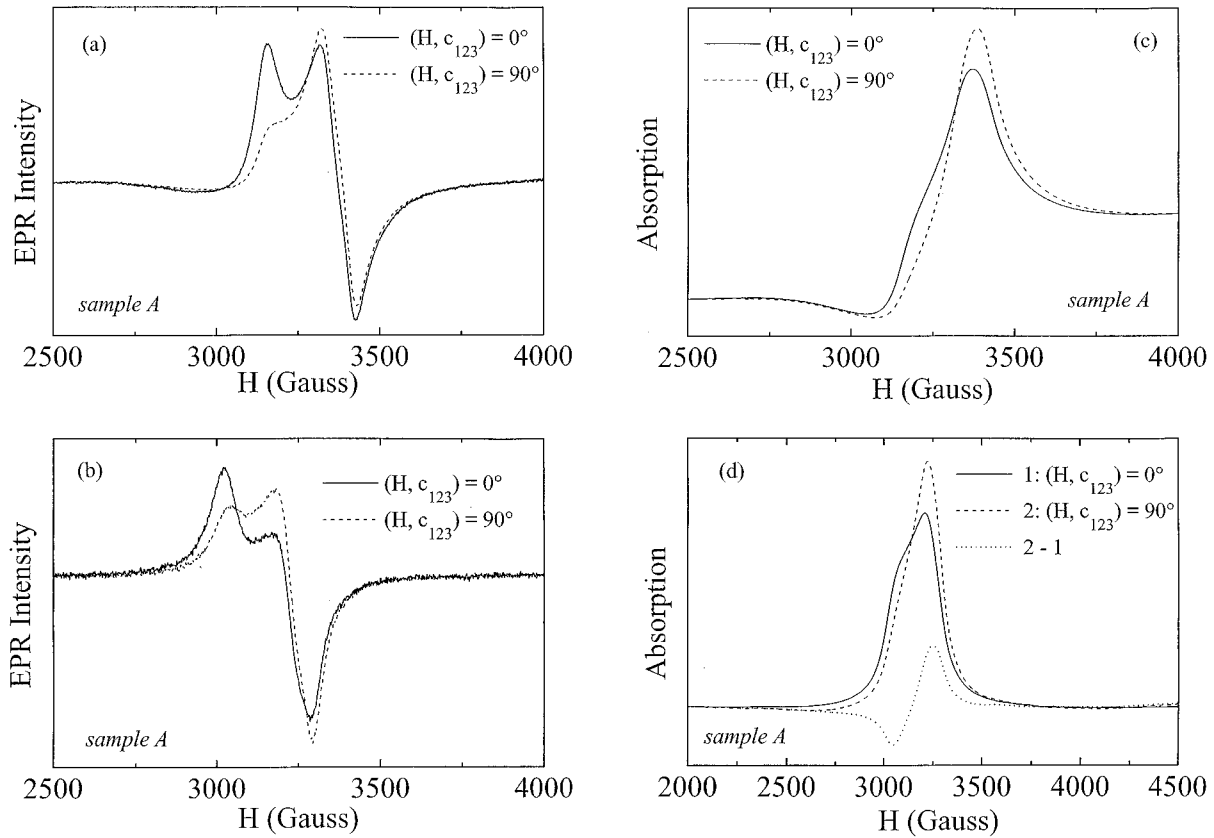


FIG. 5. Two particular spectra for sample *A* (textured under the magnetic field) taken at angles maximizing g_{\parallel} and g_{\perp} features: (a) as received and (b) deoxygenated. (c) and (d) display the corresponding integrated spectra and their difference: (c) as received and (d) deoxygenated.

5(d) (continuous line) could not be ascribed only to orthorhombicity. Furthermore, its modification by rotating along the vertical axis (dashed curve) points out a nonisotropic distribution of grains. Quantitative data only can be obtained by the relative difference as explained in Sec. II C. The negative and positive part of the difference between both curves (dotted line) are of the same area as expected since they correspond to the same spins. Using the method described previously a weight amount of $\mathcal{P}=16\%$ of oriented 211 is found.

Based on this analysis several samples were studied. Figure 6 shows the derivated spectra for sample *F* after deoxygenation. By comparing Fig. 6 to Fig. 5(b), it is obvious that a new preferential orientation is observed here, that is \mathbf{b}_{211} axis in $(ab)_{123}$ planes. This orientation amount is rather low in this sample as it concerns only 4% of 211 weight. In sample *C*, this particular orientation \mathbf{b}_{211} axis in $(ab)_{123}$ planes is observed again but now at the limit of our detection (\sim a few % 211). One sees here how sensitive this method is. Finally, the top layer of an Y_2O_3 substrate issued from the texturation experiment has been sampled for EPR investigation. It is covered by the 211 phase as a result of chemical reaction at high temperature between the peritectic liquid and Y_2O_3 .⁶ A noticeable preferential orientation of 211 is evidenced. In some cases processed differently there is no modification at all of the spectrum shape with rotation. This is the case for samples *B*, *D*, and *E*. All these results are summarized in Table I.

In brief, it is clear that 211 grains are not always isotro-

pically distributed in textured samples. When not, two orientations are evidenced: \mathbf{b}_{211} is either parallel or perpendicular to \mathbf{c}_{123} . Orientation type and amount are process dependent. In particular, substrate, thermal gradient, and magnetic field are important ingredients discussed now.

A. Texturing 211: unfavorable parameters

MgO single crystals are rather chemically inert with respect to $\text{YBa}_2\text{Cu}_3\text{O}_{7-x}$: the peritectic liquid has very small reactivity with MgO, and so this substrate is not involved in

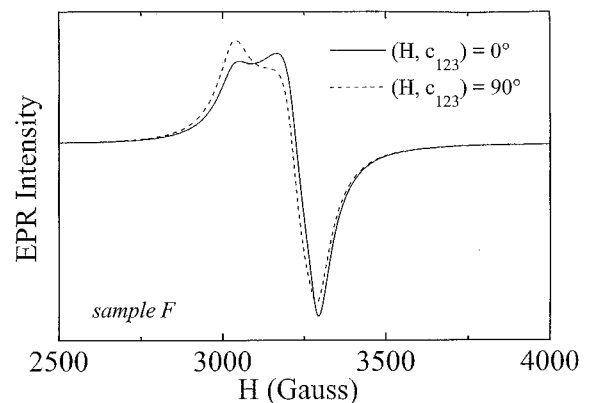


FIG. 6. Orientation dependence of EPR spectra for the sample textured on Y_2O_3 (sample *F*).

the crystallization process.^{6,24,25} Therefore it is not expected to induce any orientation of 211 as observed.

The thermal gradient is used to control the direction and progression rate of the solidification front.^{7,9,26} However, several physical and/or chemical parameters impede perfect alignment of (ab) planes: they are frequently found at 45° or even 90° from the gradient direction. This occurs for samples *B*,¹² *C*,¹⁷ and *D*. Clearly, removal of latent heat is an important factor in defining the local orientation of the solidification front. Other factors could take place too. For example, 211 grains which are entrapped in the solidification front influence the microstructure of melt-textured 123.^{26,27} Hence their orientation could compete with the general growth direction and could induce secondary nucleation, another factor inducing deviation with respect to the imposed gradient. However, in the present case there is no orientation of 211 trapped grains, this is in fact rather natural as a thermal gradient itself has no energy to orient particles except perhaps through convective forces.

B. Texturing 211: favorable parameters

The magnetic field is an external parameter the effects of which have already been presented elsewhere.^{11,12} In sample *A*, 211 orientation is due to application of a magnetic field in the high temperature part of the process. In optimized conditions (field intensity, initial composition, thermal cycle, etc.) it should be possible to orient a very high fraction of 211 grains as observed here.

It is rather surprising to find a noticeable fraction of 211 oriented grains when Y_2O_3 substrate is used: how could this substrate induce that? It has been shown that the peritectic liquid reacts with Y_2O_3 to form 211.⁶ Interestingly an oriented layer of green phase is observed by SEM at the top part of the substrate,⁶ and the present EPR results are consistent with this assumption. One supposes that, in the absence of an external parameter such as the thermal gradient or magnetic field, this 211 oriented area could act as seed for 123 crystallization. Therefore, the preferential orientation obtained for 211 inclusions in the 123 matrix on the Y_2O_3 substrate could be due to the preferred orientation of 211 issued from the reaction between the Y_2O_3 substrate and liquid. Better processing for the seed formation should increase this proportion.

The two possible 211 preferential orientations observed: $\mathbf{b}_{211} \parallel \mathbf{c}_{123}$, and $\mathbf{b}_{211} \perp \mathbf{c}_{123}$, depending on the texturation process, are compatible with a location of the 211 longest dimension, i.e., corresponding to \mathbf{a}_{211} , lying in $(ab)_{123}$ planes; see Figs. 7(a) and 7(b). In the presence of a magnetic field, due to the orientation of \mathbf{b}_{211} , oriented 211 particles necessarily have their \mathbf{a}_{211} axis in $(ab)_{123}$ planes [Fig. 7(a)]. On the other hand, the longest grain size ($|\mathbf{a}_{211}|$) in samples textured on Y_2O_3 can lie in all orientations of the plane. In the presence of the magnetic field, texturation is easier allowing a relatively high cooling rate of 3°C/h to 20°C/h .¹⁵ Then \mathbf{a}_{211} lying in $(ab)_{123}$ platelets could be a more favorable situation for 211 grains to be entrapped in the crystallization front generally perpendicular to $(ab)_{123}$ planes. We expect the orientation relationship $\mathbf{b}_{211} \parallel \mathbf{c}_{123}$ to allow a more stable growth front than when $\mathbf{b}_{211} \perp \mathbf{c}_{123}$, where several 211 grain positions are allowed with respect to 123 platelets.

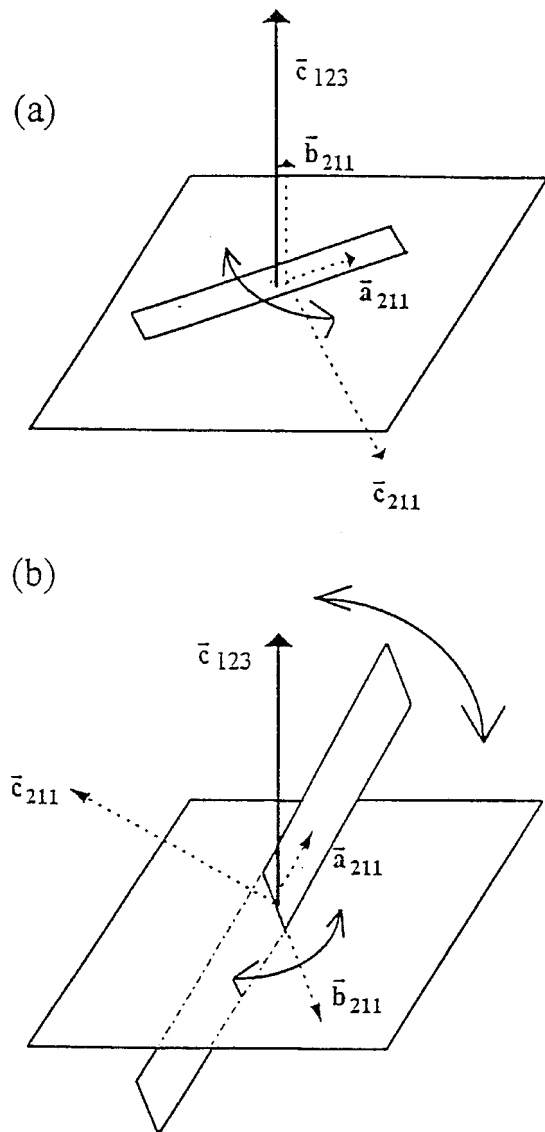


FIG. 7. Disposition of 211 grains according to the 123 platelet when (a) $\mathbf{b}_{211} \parallel \mathbf{c}_{123}$ and (b) $\mathbf{b}_{211} \perp \mathbf{c}_{123}$.

IV. CONCLUSION

A method for quantifying the ratio of 211 preferential orientation in textured YBCO materials has been established. The uncertainties due to the conducting character of the samples were strongly reduced by systematic deoxygenation of the samples. The resulting accuracy can be estimated to ± 2 in percent unit. Moreover, the extreme sensitivity of the method allows one to detect qualitatively the onset of any non-random orientation, even in a secondary phase. This type of analysis can be easily applied in other systems (nanocomposites, dispersoids, etc.), providing that the signal of the secondary phase can be clearly separated from the signal of the primary one. High- T_c cuprates are obviously favorable materials for this type of analysis due to their EPR silence.

This method has been applied to 123 textured samples with various experimental processes. It shows that a part of 211 inclusion grains is not randomly oriented. The magnetic field is particularly efficient and with 4 T, a preferential orientation $\mathbf{b}_{211} \parallel \mathbf{c}_{123}$ is obtained for 16 wt. % of 211 inclusions.

The Y_2O_3 substrate is efficient too in a smaller extent. The 211 substrate could certainly be equivalent. These two substrates allow the preferential orientation $\mathbf{b}_{211} \perp \mathbf{c}_{123}$. On the contrary, the MgO substrate and a thermal gradient are inefficient to orient 211 grains. This property of preferential orientation of 211 grains could be useful in increasing the 123 textured growth, and the magnetic superconducting properties of these textured samples.

ACKNOWLEDGMENTS

This work was supported by a cooperative program of CNRS and French Ministère de l'Enseignement Supérieur et de la Recherche Scientifique: "Supraconducteurs à Haute Température Critique pour Applications en Courants Forts" and one of us (F.J.G.) thanks the European Union for financial support (Human Capital and Mobility).

-
- ¹A. Punnoose and R. J. Singh, *Int. J. Mod. Phys. B* **9**, 1123 (1995).
²S. Chakravarty and R. Orbach, *Phys. Rev. Lett.* **64**, 224 (1990).
³P. Simon, J. M. Bassat, S. B. Oseroff, Z. Fisk, S. W. Cheong, A. Wattiaux, and S. Schultz, *Phys. Rev. B* **48**, 4216 (1993).
⁴N. Guskos, V. Likodimos, C. A. Londos, V. Psycharis, C. Mitros, A. Koufoudakis, H. Gamari-Seale, W. Windsch, and H. Metz, *J. Solid State Chem.* **119**, 50 (1995).
⁵T. Kobayashi, H. Katsuda, K. Hayashi, M. Tokumoto, and H. Ihara, *Jpn. J. Appl. Phys.* **27**, L670 (1988).
⁶N. Pellerin, P. Odier, P. Simon, and D. Chateigner, *Physica C* **222**, 133 (1994).
⁷S. Jin, T. H. Tiefel, R. C. Sherwood, R. B. Van Dover, M. E. Davis, G. W. Kammlott, and R. A. Fastnacht, *Phys. Rev. B* **37**, 7850 (1988).
⁸M. Murakami, M. Morita, K. Doi, and V. Mugamoto, *Jpn. J. Appl. Phys.* **28**, 1189 (1989).
⁹K. Salama and D. F. Lee, *Supercond. Sci. Technol.* **7**, 177 (1994).
¹⁰F. J. Gotor, J. Ayache, N. Pellerin, and P. Odier, *J. Mater. Res.* (to be published).
¹¹N. Pellerin, F. J. Gotor, P. Simon, L. Durand, and P. Odier, *Solid State Commun.* **96**, 721 (1995).
¹²L. Durand, F. Kircher, P. Regnier, D. Chateigner, N. Pellerin, F. J. Gotor, P. Simon, and P. Odier, *Supercond. Sci. Technol.* **8**, 214 (1995).
¹³J. Ayache, P. Odier, and N. Pellerin, *Supercond. Sci. Technol.* **7**, 655 (1994).
¹⁴D. E. Farrel, B. S. Chandrasekhar, M. R. de Guire, M. M. Fang, V. G. Kogan, R. Clem, and D. K. Finnemore, *Phys. Rev. B* **36**, 402 (1987).
¹⁵P. de Rango, M. Lees, P. Lejay, A. Suplice, R. Tournier, M. Ingold, M. Germe, and M. Pernet, *Nature* **349**, 770 (1991).
¹⁶L. Durand, Thèse de l'université Pierre et Marie Curie Paris, France, 1995.
¹⁷I. Monot, M. Lepropre, J. Provost, G. Desgardin, B. Raveau, D. Bourgault, J. M. Barbut, D. Braithwaite, and R. Tournier, *Supercond. Sci. Technol.* **5**, 712 (1992).
¹⁸J. F. Dyson, *Phys. Rev.* **98**, 349 (1955).
¹⁹G. Feher and A. F. Kip, *Phys. Rev.* **98**, 337 (1955).
²⁰G. E. Pake and E. M. Purcell, *Phys. Rev.* **74**, 1184 (1948).
²¹G. E. Pake and E. M. Purcell, *Phys. Rev.* **75**, 534 (1949).
²²F. Hanic, G. Plesch, S. Buchta, J. Dobrovodsky, and L. Danielik, *J. Solid State Chem.* **116**, 136 (1995).
²³A. Douy and P. Odier, *Mater. Res. Bull.* **24**, 1119 (1989).
²⁴N. Pellerin, M. Gervais, and P. Odier, in *Layered Superconductors: Fabrication, Properties and Applications*, edited by D. T. Shaw *et al.*, MRS Symposia Proceedings No. 275 (Materials Research Society, Pittsburgh, 1992), p. 537.
²⁵N. Pellerin, P. Simon, P. Odier, D. Chateigner, P. Germe, M. Pernet, and J. P. Bonnet, in *Superconductivity*, edited by C. W. Chu *et al.*, ICMAS 92 (IITT, 1992), p. 99.
²⁶P. Diko, W. Gawalek, T. Habisreuther, T. Klupsch, and P. Gornert, *Phys. Rev. B* **13**, 658 (1995).
²⁷G. J. Schmitz, J. Laakmann, Ch. Walters, and S. Rex, *J. Mater. Res.* **8**, 2774 (1993).